Journal of Microscopy, Vol. 186, Pt 3, June 1997, pp. 212–220.
Received 15 August 1996; accepted 14 January 1997

Double-pulse fluorescence lifetime measurements

A. H. BUIST,* M. MÜLLER,* E. J. GIJSBERS,* G. J. BRAKENHOFF,* T. S. SOSNOWSKI,† T. B. NORRIS† & J. SQUIER‡

**BioCentrum Amsterdam, University of Amsterdam, Department of Molecular Cytology, Kruislaan 316, 1098 SM Amsterdam, The Netherlands*

†Center for Ultrafast Optical Science, University of Michigan, 2200 Bonisteel Blvd, IST Building, Ann Arbor, MI 48109–2099, U.S.A.

‡Department of Electrical and Computer Engineering, University of California, San Diego, Urey Hall, Mail Code 0339, La Jolla, CA 92093–0339, U.S.A.

Key words. CCD, confocal microscopy, fluorescence relaxation, fluorescence, lifetime imaging, saturation.

Summary

It is demonstrated that fluorescence lifetimes in the nanosecond and picosecond time-scale range can be observed with the recently proposed double-pulse fluorescence lifetime imaging technique (Müller *et al.*, 1995, Double-pulse fluorescence lifetime imaging in confocal microscopy. *J. Microsc.* **177,** 171–179).

A laser source with an optical parametric amplifier (OPA) system is used to obtain short pulse durations needed for high time resolution, wavelength tunability for selective excitation of specific fluorophores and high pulse energies to obtain (partial) saturation of the optical transition.

It is shown that fluorescence lifetimes can be determined correctly also with nonuniform saturation conditions over the observation area.

A correction scheme for the effect on the measurements of laser power fluctuations, which are inherently present in OPA systems, is presented. Measurements on bulk solutions of Rhodamine B and Rhodamine 6G in different solvents confirm the experimental feasibility of accessing short fluorescence lifetimes with this technique.

Because signal detection does not require fast electronics, the technique can be readily used for fluorescence lifetime imaging in confocal microscopy, especially when using bilateral scanning and cooled CCD detection.

Correspondence to: A. H. Buist. Tel: (31)-20-5256225; fax: (31)-20-5256271; email: buist@mc.bio.uva.nl

1. Introduction

Measurement of fluorescence lifetimes* facilitates a variety of detailed studies on the kinetics of intra- and intermolecular processes. For example, the sensitivity of the fluorescence lifetime of fluorescent dyes to the local pH (Lippitsch *et al.*, 1992; Draxler *et al.*, 1993), presence of oxygen (Lakowicz, 1980) or concentration of particular ions (Lakowicz & Szmacinski, 1993; Sanders *et al.*, 1994) makes fluorescence lifetime measurement an important tool for investigating biochemistry at the molecular level. Detailed knowledge of fluorescence lifetimes is also required for analysing anisotropy decay data. From such data inferences on, for example, the local viscosity, shape and flexibility of macromolecules can be made (e.g. Steiner, 1991).

To date there are two main techniques for measuring fluorescence lifetimes (Anderson, 1991). The first technique is the pulse method where the fluorescence intensity following a short excitation pulse is observed in time using photon counting and correlation techniques. The second technique is the phase-modulation method, where the lifetimes are calculated from the relative phase and amplitude of the fluorescence intensity with respect to a sinusoidally modulated excitation field.

Both methods are well established and in principle can provide the same information, although there are circumstances where one technique is preferable over the other. A common aspect of both techniques is the limited time resolution imposed by the response time of the detector chain. For both techniques the ultimate time resolution is on the order of several tens of picoseconds, but achieving this takes considerable technical and mathematical effort (e.g. Straume *et al.*, 1991) and also considerable measurement time.

*By convention, the (partly) fluorescent depopulation of an excited state as a function of time is described by one or more characteristic decay parameters, the fluorescence lifetimes. Most often these lifetimes are the 1/e-times figuring in a multi-exponential model of the temporal behaviour of the fluorescence intensity.

Incorporation of fluorescence lifetime measurements within fluorescence microscopy potentially has great benefits, since the molecular kinetics can then be observed with both high temporal and spatial resolution. Indeed several proposals for fluorescence lifetime imaging have been reported (e.g. Lakowicz & Berndt, 1991), but practical limitations restrict the resolution that can be obtained with the above-mentioned techniques in a fluorescence microscope to be of the order of 0·5–1 ns (Gadella *et al.*, 1994; Sanders *et al.*, 1994; So *et al.*, 1995).

In the present contribution we describe fluorescence lifetime measurements using the recently proposed double-pulse fluorescence lifetime imaging (DPFLIm) technique (Müller *et al.*, 1995). In this method, a pump pulse (partially) saturates the optical transition of fluorescent molecules in a sample. The time-integrated fluorescence intensity obtained after a second – probe – pulse depends via the various decay parameters on the delay time between pump and probe pulse. The time resolution, when employing very short (tens of femtoseconds) pulses, is determined by the delay time between the two pulses. Delay lines that allow variation of the pathlength with micrometre precision are readily available, bringing in principle subpicosecond time scales within range. Because signal detection and extraction of fluorescence lifetimes is both fast and simple, incorporation within (confocal) fluorescence microscopy is straightforward with this technique.

For the experiments reported here, optical pulses are focused under low numerical aperture (NA) conditions in a bulk fluorophore solution. The first pulse creates a spatially varying degree of optical saturation which is subsequently probed by the second pulse. Owing to the pulsed nature of the excitation, the emitted fluorescence signal will be a short and intense burst of photons which is difficult to detect linearly with photomultipliers. Collection of (part of) the fluorescence photon burst on a CCD detector ensures an efficient linear detection. This method of detection constitutes a spatial integration over volume elements with different degrees of optical saturation. As will be shown, fluorescence lifetimes can be extracted without uniformity in optical saturation.

In the experiments reported here, the optical parametric amplifier (OPA) output power fluctuations were of the order of 10%, and determination of the fluorescence lifetimes requires that one corrects for these fluctuations. A correction scheme is presented with which it is possible to correct for the effect these power fluctuations have on the measurements. After correction, the fluorescence lifetimes can be extracted without difficulty.

The organization of this paper is as follows. In Section 2 the experimental set-up is given, together with a basic description of the method. In Section 3 the effect of spatial integration over volumina with different degrees of optical saturation is examined, based on a two-level excitation model, leading to a simple way of extracting the fluorescence lifetimes. The correction scheme for laser power fluctuations is covered in Section 4. Some experimental results are shown in Section 5.

2. Experimental set-up and basic description of the method

Experimental set-up

The experimental set-up is shown schematically in Fig. 1.

The OPA system (Sosnowski *et al.*, 1996) delivers linearly polarized optical pulses of ≈ 30-fs duration, with an energy of 1–5 nJ at a repetition rate of 250 kHz and at wavelengths tunable from 450 to 700 nm. The OPA is pumped by the frequency-doubled output of an 800-nm Ti:sapphire regenerative amplifier, which is also used to generate a white-light continuum from which the signal pulse is selected. These laser pulses have sufficient energy to realize partial saturation conditions when focused, under low NA conditions, in a bulk fluorophore solution (Ghauharali *et al.*, 1997). The repetition rate is sufficiently low to have negligible pile-up effects (Müller *et al.*, 1995) for the fluorophore solutions under consideration here.

After passing a BG39 filter to block pump laser light, the beam is collimated by a slightly magnifying telescope. The parallel beam (≈ 3 mm full width half-maximum beam diameter) is directed towards a 50% beamsplitter which divides the beam into two beams, to be denoted by object and reference beam. The object and reference beams are both reflected by a retroreflector and, after passing the beamsplitter for the second time, are directed parallel and collinear towards the 30-mm focusing lens. The retroreflector in the object beam is positioned on a variable delay

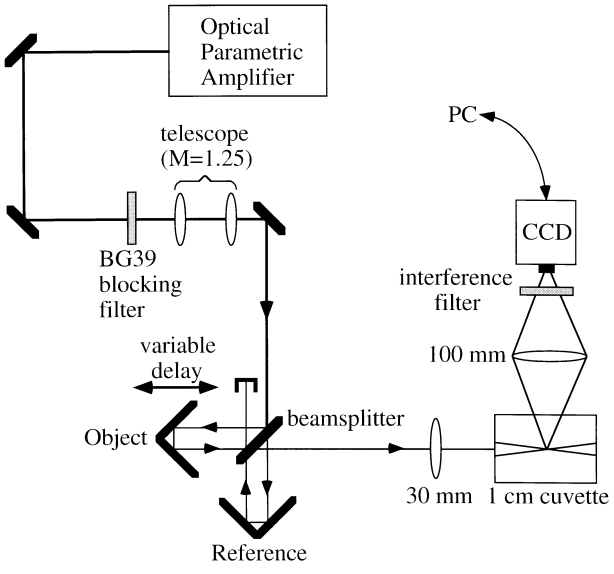

Fig. 1. Schematic layout of the experimental set-up.

line which is adjustable over a 135-cm distance range with a precision of better than 1 mm. Thus the delay time between the two pulses is adjustable over a range of 9 ns with a precision of about 7 ps. With the 30-mm lens the beams are focused in a 1-cm cuvette containing a fluorophore solution. The fluorescence generated in the fluorophore solution is imaged (1:1, perpendicular to the propagation direction of the excitation light) onto a cooled CCD camera (768 by 512 square pixels of 9-μm width) with a 100-mm lens. The interference filter in front of the CCD camera prevents scattered excitation photons contributing to the image. The camera is controlled by a PC that is also used for image read-out and storage.

Basic description of the method

In Fig. 2, the cuvette and the fluorescence generated by focusing the light (propagating along the Z-axis) in the fluorophore solution are depicted schematically.

When the energy per pulse is low and saturation of the optical transition does not occur, the total time-integrated fluorescence generated in a thin slab (dZ) perpendicular to the Z-axis, as indicated in Fig. 2, is independent of the position along the Z-axis. The reason for this is that, even in the focal region, only a small fraction of fluorophores is excited. Hence the number of excited fluorophores is directly proportional to the total number of excitation photons passing through the slab. This number is independent of Z-position provided that absorption and scattering are very small.

When the energy per pulse is increased, the optical transition from the ground state to the excited state will start to saturate, at first in the focal region. Consequently, the total time-integrated fluorescence generated in slabs with significant saturation – i.e. in and around focus – will be less than the total time-integrated fluorescence generated in slabs with no saturation – i.e. far from focus.

If we now consider a slab with significant average saturation per pulse and perform a double pulse experiment (Müller *et al.*, 1995) it is seen that the total time-integrated fluorescence generated in the slab will increase with increased delay time between the two pulses: some of the fluorophores that were excited by the first pulse will have relaxed to the ground state, the probability of relaxation increasing with delay time, prior to arrival of the second pulse. Some of these fluorophores will again be excited and thus cause an increase in total fluorescence with delay time. This delay time dependence of the total time-integrated fluorescence is shown schematically in Fig. 3. The DPFLIm technique uses the increase in total time-integrated fluorescence as a function of delay time between the two pulses to obtain the fluorescence lifetimes.

In the experimental set-up (Fig. 1) the fluorescence generated in the cuvette is projected onto the CCD camera. This means that the fluorescence generated in a volume is integrated on a CCD pixel. As will be shown in the next section, the fluorescence lifetimes can be extracted without requiring uniformity in optical saturation throughout the integrated volume. This is a key feature for the determination of fluorescence lifetimes from the total time-integrated fluorescence in a thin slab perpendicular to the Z-axis as shown in Fig. 2. These total time-integrated fluorescence values as a function of Z-position are obtained by integrating, perpendicular to the optical axis, all pixels belonging to the same column of the CCD camera. As will be shown in Section 4, these plots of total time-integrated fluorescence as a function of Z-position provide a good starting point for correction of the effect on the measurements of laser power fluctuations.

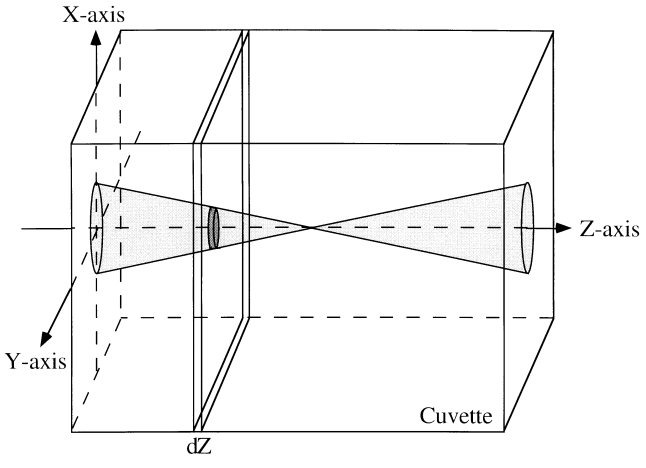

Fig. 2. The excitation light travelling along the Z-axis is focused, under low NA conditions, in a fluorophore solution.

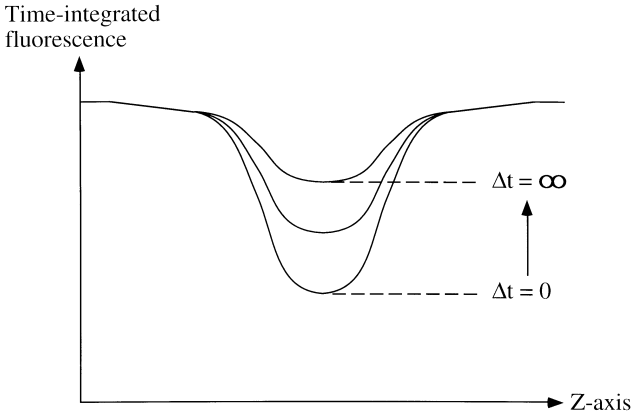

Fig. 3. The total time-integrated fluorescence in a thin slab perpendicular to the Z-axis, as a function of Z-position. In areas where saturation occurs, the total time-integrated fluorescence for a double-pulse experiment will increase with the delay time between the pulses.

3. Modelling of excitation-decay mechanism

With an isotropically orientated ensemble of fluorophores for which the quasistationary excitation (Schubert & Wilhelmi, 1986) can be described by a two-level system, the number of excited fluorophores at time t (s) in a volume element dV (m^3) is given (Loudon, 1973) by

$$n_1(t)\mathrm{d}V = \left\{\frac{BW}{A+2BW}n + \left(n_1(0) - \frac{BW}{A+2BW}n\right)e^{-(A+2BW)t}\right\}\mathrm{d}V. \quad (1)$$

where n (m^{-3}) is the total fluorophore density, n_1 (m^{-3}) is the excited state fluorophore density, A (s^{-1}) is the Einstein coefficient of spontaneous emission (also called the fluorescence decay rate), B (m^3 J^{-1} s^{-2}) is the Einstein coefficient of stimulated emission (equal to the Einstein coefficient of absorption) and W (J.s m^{-3}) is the energy density, divided by the spectral bandwidth, of the excitation field in volume element dV. The total fluorophore density n is assumed to be independent of position in the cuvette. It is assumed that volume element dV is small enough to take W constant throughout dV. It is also assumed that photodegradation of the fluorophores is negligible. The last assumption is reasonable for the present experimental set-up because thermal diffusion refreshes the excited volume sufficiently fast. A simple back-of-the-envelope calculation will show that this is indeed realistic: if we accept that we need about 10^5 excitations to degrade a fluorophore molecule (Sandison *et al.*, 1995) then, since the pulses are very short relative to the fluorescent lifetime (thus giving no more than 1 excitation per pulse, per fluorophore molecule), at 250 kHz repetition rate the same molecule must reside no longer than 0·4 s within the saturated focal region. In 0·4 s a typical dye molecule in water will diffuse over about 20 μm (Sandison *et al.*, 1995), which is sufficient to refresh the focal region (approx. diameter of 12 μm (Ghauharali *et al.*, 1996).

For a very short pulse with pulse duration t_p (s) $<< A^{-1}$, spontaneous emission during t_p and the temporal profile of W can be neglected. The number of excited fluorophores in volume element dV immediately after the pulse, starting at $t = 0$, then follows from Eq. (1) (with $BW >> A$) as

$$n_1(t_\mathrm{p})\mathrm{d}V = \left\{\frac{n}{2} + \left(n_1(0) - \frac{n}{2}\right)e^{-2BWt_\mathrm{p}}\right\}\mathrm{d}V. \quad (2)$$

The subsequent decay in the absence of an exciting field and valid for $t \geq t_\mathrm{p}$ reads

$$n_1(t)\mathrm{d}V = \left\{n_1(t_\mathrm{p})e^{-A(t-t_\mathrm{p})}\right\}\mathrm{d}V. \quad (3)$$

Using Eqs. (2) and (3) the time dependence of fluorophore densities in the ground state (n_0) and excited state (n_1), in volume element dV for a double pulse experiment, can be described (Table 1). In writing out this scheme, differences in pulse duration and pulse energy for the object and reference pulse are allowed for because these differences may be introduced by the slight asymmetry between object and reference beam (see Fig. 1). In Table 1 the first pulse starts at $t = 0$ and ends at $t = t_{\mathrm{p}1}$. Δt seconds later the second pulse starts ($t = t_{\mathrm{p}1} + \Delta t$) and ends at $t = t_{\mathrm{p}1} + t_{\mathrm{p}2} + \Delta t$. At $t = \infty$ the system has relaxed to the starting situation. In Table 1 a shorthand notation is used, where

$$w_1 = e^{-2BW_1 t_{\mathrm{p}1}},\ w_2 = e^{-2BW_2 t_{\mathrm{p}2}} \text{ and } a = e^{-A\Delta t}.$$

Using Table 1, the time-integrated fluorescence (TIF) originating from volume element dV for excitation with only the first pulse present can be written as

$$\mathrm{TIF}_1 = f\frac{n}{2}\{1 - e^{-2BW_1 t_{\mathrm{p}1}}\}\mathrm{d}V \quad (4)$$

and similarly for excitation with only the second pulse present

$$\mathrm{TIF}_2 = f\frac{n}{2}\{1 - e^{-2BW_2 t_{\mathrm{p}2}}\}\mathrm{d}V, \quad (4a)$$

where f is a proportionality factor accounting for the quantum yield of the fluorophore and the detection efficiency of the set-up. For double-pulse excitation with delay time Δt between the pulses, the time-integrated fluorescence follows from Table 1, using Eqs. (4) and (4a), as

$$TIF_{1+2}(\Delta t) = \mathrm{TIF}_1 + \mathrm{TIF}_2 - f\frac{n}{2}e^{-A\Delta t}\left\{(1 - e^{-2BW_2 t_{\mathrm{p}2}})(1 - e^{-2BW_1 t_{\mathrm{p}1}})\right\}\mathrm{d}V. \quad (5)$$

Integration of Eq. (5) in X- and Y-direction over the dimensions of the cuvette yields the total time-integrated

Table 1. Time dependence of fluorophore densities in the ground state (n_0) and exited state (n_1) for double pulse excitation, when using very short pulses.

t	n_0	n_1
0	n	0
$t_{\mathrm{p}1}$	$\{1 + w_1\}\frac{n}{2}$	$\{1 - w_1\}\frac{n}{2}$
$t_{\mathrm{p}1} + \Delta t$	$(2 - a\{1 - w_1\})\frac{n}{2}$	$a\{1 - w_1\}\frac{n}{2}$
$t_{\mathrm{p}1} + t_{\mathrm{p}2} + \Delta t$	$(\{1 + w_2\} - aw_2\{1 - w_1\}\frac{n}{2}$	$(\{1 - w_2\} + aw_2\{1 - w_1\})\frac{n}{2}$
∞	n	0

fluorescence for a slab, between Z and Z + dZ, perpendicular to the Z-axis:

$$\int_{X,}\int_{Y}\mathrm{TIF}_{1+2}(\Delta t)=\int_{X,}\int_{Y}\mathrm{TIF}_{1}+\int_{X,}\int_{Y}\mathrm{TIF}_{2}-f\frac{n}{2}e^{-A\Delta t}\mathrm{d}Z\int_{X,}\int_{Y}\times(1-e^{-2BW_{2}t_{p2}})(1-e^{-2BW_{1}t_{p1}}). \quad (6)$$

Note that, since fluorescence decay rate A is independent of position for a homogeneous fluorophore solution, it can be taken outside the integration. Hence even without uniformity in excitation intensity throughout the integrated volume and hence without uniformity in optical saturation, fluorescence decay rate A can be obtained from the experimental data, consisting of the time-integrated fluorescence for both pulses separately and the time-integrated fluorescence at several different Δt values between the two pulses. Another important aspect of Eq. (6) is that fluorescence decay rate A can only be extracted reliably when the double integral in the last term of in Eq. (6) is significantly larger than 0, i.e. a significant degree of saturation is required.

The model used to derive Eq. (6) is a simplified one in two related respects.

First, the assumption that there is only one fluorescence decay rate (A) need not be true for fluorophores that interact with their environment. Multiexponential and nonexponential decay mechanisms can then occur. In the latter case it is, however, always possible to expand the decay in multiexponential form (Lakowicz, 1983). Multiexponential decays can be incorporated in Eq. (6) without difficulty, and hence are still obtainable without requiring uniformity in optical saturation throughout the integrated volume.

Second, the model does not allow for more than two energy levels. It can be shown (forthcoming publication) that for more than two energy levels, e.g. when including rovibrational relaxation pathways, the decay parameters can still be extracted without uniformity in optical saturation throughout the integrated volume.

4. Correction for power fluctuations

A practical complication in extracting fluorescence lifetimes using Eq. (6) from the previous section arises when the output power of the laser varies during the experiment. These power fluctuations cause all terms in Eq. (6) to vary in time, (partly) obscuring the effect of delay time Δt on the change in time-integrated fluorescence.

As was stated in Section 2, the total time-integrated fluorescence, in thin slabs perpendicular to the Z-axis and as a function of Z-position, can be employed to correct for the effect of laser power fluctuations. This correction procedure will be explained in this section.

In Fig. 4 the total time-integrated fluorescence as a function of Z-position is given for three repeated measurements, i.e. at the same delay time between the two pulses. The cuvette contained a dilute solution (10^{-7} m) of RhB in methanol; the excitation wavelength was 555 nm. The integration time per measurement was 10 s, meaning that at a repetition rate of 250 kHz, 2·5 million pulse-pairs were used in each measurement of the total time-integrated fluorescence. Fast pulse-to-pulse fluctuations will effectively be averaged, but a slower variation of about 10% in average laser power is showing up in Fig. 4.

To correct for the effect of average power fluctuations analytically, using Eq. (6) from the previous section, requires precise knowledge of the average power of both object and reference beam as well as precise knowledge of the energy density distribution throughout the volume from which the time-integrated fluorescence is obtained.

A more pragmatic approach to the problem, which does not require any knowledge about the energy density distribution throughout the excited volume, is the following.

From the plots in Fig. 4 it is clear that far from the focal region the total time-integrated fluorescence becomes independent of the Z-position. These areas show no significant saturation of the optical transition and thus the fluorescence far from the focal region is a direct, linear, measure of the total excitation power. In the focal region the effect of saturation is clearly visible as a dip in the integrated fluorescence. Owing to the nonlinear character of optical saturation as a function of excitation energy density, it is not possible (unless, as stated before, the energy density distribution throughout the excited volume is known) to use the measured total excitation power, obtained from unsaturated regions, to directly compensate

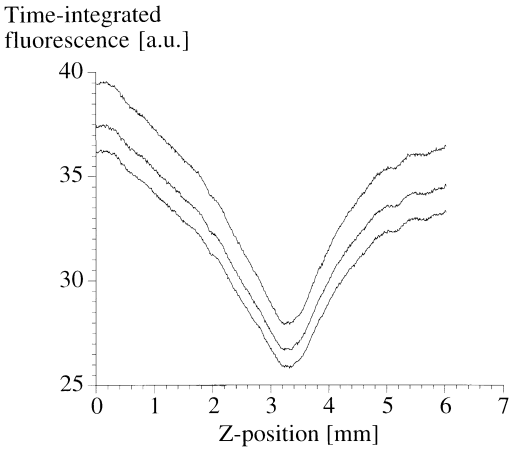

Fig. 4. Repeated measurements of total time-integrated fluorescence as a function of Z-position (the light pulses travel in the Z-direction). The difference in total time-integrated fluorescence between the entrance and exit planes indicates a small excitation light depletion (about 5%) due to scattering and absorption.

for power-effects on the time-integrated fluorescence in regions where saturation occurs. If, however, the average power variations are not too large, the nonlinear behaviour of optical saturation as a function of excitation energy density may well be approximated by a linear function, as schematically depicted in Fig. 5.

From the linear interpolation the correct time-integrated fluorescence at some desired target entry power level can be estimated. The slope of the line that best fits the experimental data will, of course, depend on the Z-position since it reflects the average degree of optical saturation over the integrated volume, and it will also depend on the delay time between the pulses.

In practice this correction procedure works well, as will be demonstrated in the next section. All measurements at certain delay time Δt are repeated a few (3–6) times and, by using the procedure described above, are all corrected to yield the time-integrated fluorescence at the target entry power level. Usually this target entry power level will be the average entry power level over the complete series of measurements. After this correction the fluorescence lifetimes are easily obtained since now the last double integral in Eq. (6), at some Z-position, is a constant throughout the full Δt series.

5. Experiments

In Fig. 6 a typical measurement series of the total time-integrated fluorescence as a function of Z-position and for several different delay times between the pulses is shown. The cuvette contained a dilute solution (10^{-7} m) of RhB in methanol, which was excited at 555 nm. The integration time per measurement was 10 s, the delay time varied from $-0{\cdot}3$ to $8{\cdot}6$ ns. Here negative times indicate that the optical pathlength in the object branch is shorter than the optical pathlength in the reference branch (Fig. 1). Also the sum of total time-integrated fluorescence as a function of Z-position taken with reference and object pulse separately (thus effectively $\Delta t = \infty$) is included in Fig. 6. Clearly the effect of delay time on the change in time-integrated fluorescence is severely masked by the power fluctuations of the excitation.

The full measurement shown in Fig. 6 was repeated three times. Then the correction scheme described in the previous section was applied to the data, yielding the result depicted in Fig. 7.

Plotting the total time-integrated fluorescence, averaged over a Z-range of 2 mm around the minimum value, as a function of Δt yields the result given in Fig. 8. This averaging range of 2 mm has been chosen because over this range a significant systematic variation in total time-integrated fluorescence with delay time Δt is observed in Fig. 7. As can be inferred from Eq. (6) this averaging does not affect the calculated fluorescence decay rate A other than that it improves the signal-to-noise ratio (SNR). At $8{\cdot}6$ ns delay time, the total time-integrated fluorescence was found to be at more than 99·9% of the limiting value ($\Delta t = \infty$) obtained by summing the total time-integrated fluorescence as a function of Z-position taken with reference and object pulse separately.

From Eq. (6) it is readily derived that fluorescence decay rate A can be obtained from

$$\ln\left(\int_X\int_Y\int_Z \mathrm{TIF}_1 + \int_X\int_Y\int_Z \mathrm{TIF}_2 - \int_X\int_Y\int_Z \mathrm{TIF}_{1+2}(\Delta t)\right) = -A\Delta t + \ln\left(f\frac{n}{2}\int_X\int_Y\int_Z (1 - e^{-2BW_2 t_{p2}})(1 - e^{-2BW_1 t_{p1}})\right) \quad (7)$$

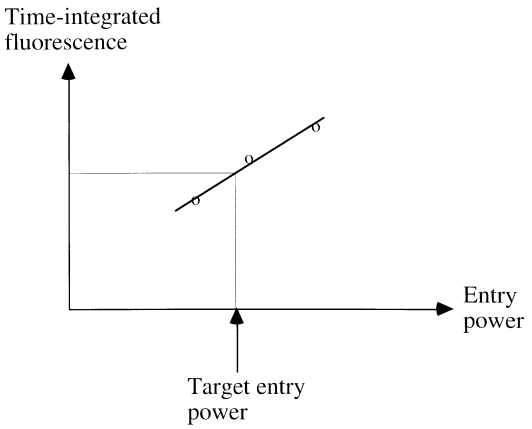

Fig. 5. Linear interpolation through time-integrated fluorescence data, at the same Z-position and at the same delay time between the pulses, obtained at different entry power levels, can be used to estimate the true time-integrated fluorescence at a desired target entry power level at this Z-position and delay time.

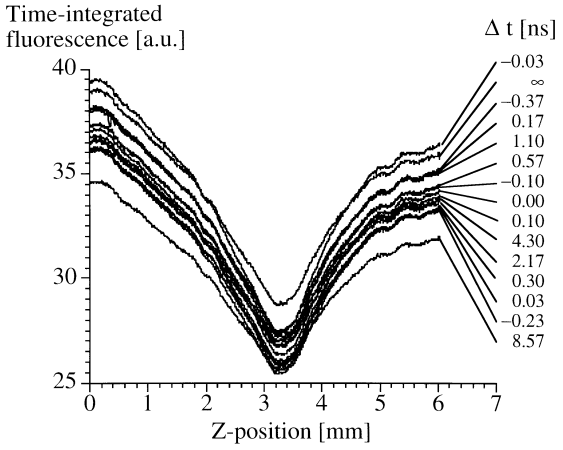

Fig. 6. Measurements of total time-integrated fluorescence as a function of Z-position (the light pulses travel in the Z-direction), for 15 different Δt values. Negative times indicate that the optical path length in the object branch is shorter than the optical path length in the reference branch (Fig. 1).

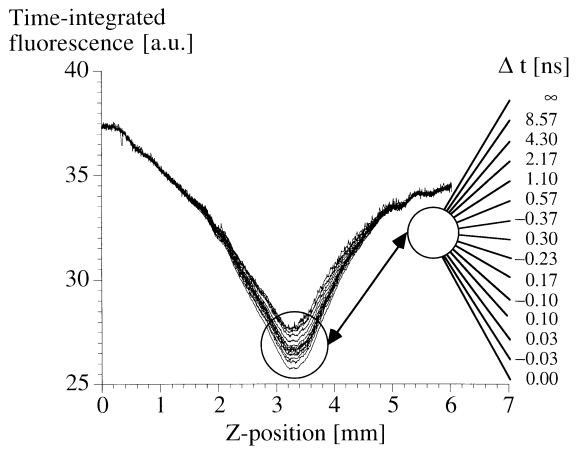

Fig. 7. The same data as depicted in Fig. 6, after correction for laser power fluctuations.

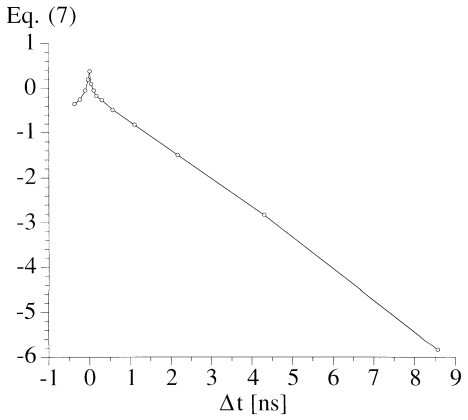

Fig. 9. Left-hand side of Eq. (7) calculated for the experimental data shown in Fig. 8. From the slope at the larger delay times (least-squares fit for $\Delta t > 1$ ns) a fluorescence lifetime of $1{\cdot}49 \pm 0{\cdot}03$ ns is obtained.

i.e. as a function of Δt, the logarithm given in the left-hand side of Eq. (7) yields a straight line with slope $-A$. Insertion of the experimental data in Eq. (7) yields the plot shown in Fig. 9. Fitting a straight line through the data points obtained at the larger Δt values ($\Delta t > 1$ ns) yields a fluorescence lifetime of $1{\cdot}49 \pm 0{\cdot}03$ ns. From the behaviour at smaller Δt values shown in Fig. 9 it is seen that a single exponential decay does not fully describe the observed data. If a bi-exponential curve given by

$$\text{total time-integrated fluorescence} = a - be^{\frac{-\Delta t}{\tau_1}} - ce^{\frac{-\Delta t}{\tau_2}} \quad (8)$$

is fitted (least-squares fit, for $\Delta t > 0$) to the data depicted in Fig. 8 we find $\tau_1 = 1{\cdot}4 \pm 0{\cdot}1$ ns and $\tau_2 = 0{\cdot}03 \pm 0{\cdot}01$ ns, respectively.

Similar bi-exponential fits have been made to experimental data obtained for various fluorochrome/solvent combinations. RhB was excited at 555 nm, Rh6G at 529 nm, with the wavelengths selected by appropriate tuning of the OPA system. Otherwise identical experimental conditions as described before were used. The results are summarized in Table 2.

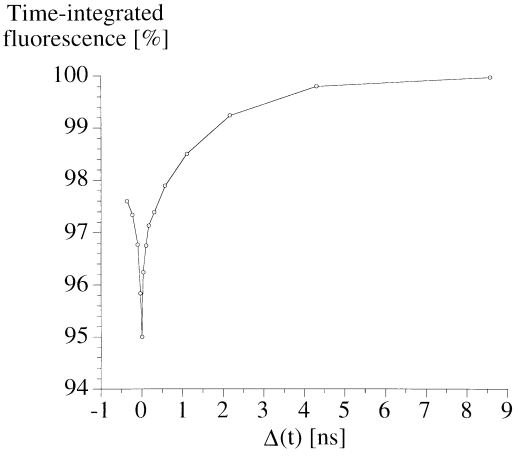

Fig. 8. Measured relation between the total time-integrated fluorescence, averaged over a Z-range of 2 mm around the focal saturation region (see text) and expressed as a percentage of the limiting value obtained for $\Delta t = \infty$, and delay time Δt.

When the τ_1 values from Table 2 are compared with fluorescence lifetimes measured with standard measurement techniques it is seen that the results obtained with the DPFLIm method are consistent, except for the case of Rh6G in water. This discrepancy is caused by over-correction for laser power fluctuations for the $\Delta t = \infty$ data. As can be inferred from Section 4, extrapolation either side beyond the range of validity of the linear approximation will lead to over-correction for laser power fluctuations.

The τ_2 component which is about two orders of magnitude smaller than the fluorescence lifetimes is probably due to fast rotational modes which can occur at this time scale (Gumy & Vauthey, 1996). Rotational modes are expected to be visible with the experimental set-up used, since linearly polarized light is used. Another possibility is that vibrational relaxation is the cause of the fast decay component.

6. Discussion and conclusion

As demonstrated in this paper, it is possible to measure fluorescence lifetimes at nanosecond and subnanosecond time-scales using the DPFLIm method.

The possibility to obtain the lifetimes without requiring uniformity in optical saturation and the procedure to correct for laser power fluctuations make the method experimentally feasible. However, the precision of the measurements is at present limited by the OPA output power fluctuations that are left uncorrected by the linear correction procedure. More elaborate correction procedures

Table 2. Summary of measured decay parameters for various fluorophore/solvent combinations.

Solution (all 10^{-7} M)	τ_1 (ns)	Literature value (ns)	τ_2 (ns)
Rh6G in water	6·5 ± 1·0	4 (Lakowicz & Berndt, 1993)	0·30 ± 0·10
Rh6G in ethanol	3·9 ± 0·5	3·9 (Gumy & Vauthey, 1996)	0·11 ± 0·03
RhB in water	1·8 ± 0·7	1·5 (Lakowicz & Berndt, 1993)	0·26 ± 0·13
RhB in methanol	1·4 ± 0·1	—	0·03 ± 0·01

or preferably more stable OPA systems are therefore essential for further improvement in precision.

Since data extraction, after correction for laser output power variation, is both fast and simple, incorporation of this method within a confocal microscopy setting is possible without sacrificing time resolution.

In the confocal microscope, every point of interest is illuminated under high NA conditions. The fluorescence of this point is collected, under high NA conditions and through a detector pinhole, on a CCD detector (Brakenhoff & Visscher, 1992, 1993). Measuring, at the same point, the increase in total time-integrated fluorescence for several Δt values allows us to measure the fluorescence decay parameters at this point. The combination of a high NA objective lens for excitation and detection and the detector pinhole will ensure good 3D confocal resolution, only moderately diminished by the increased level of excitation needed to obtain (partial) saturation of the optical transition (Visscher *et al.*, 1994). The repetition rate used for the experiments reported in the present paper (250 kHz), as argued in Section 3, is low enough to have negligible photobleaching (due to diffusion) within the saturated focal region. In a confocal microscope operated in point-scanning mode, a repetition rate of 250 kHz may be too low, but in line-scanning mode 250 kHz will be sufficient. However, if the photobleaching problem is addressed properly by using a beam blanker, the upper limit in usable repetition rate is given by the fluorescent lifetimes of the sample: if the longest lifetime is, for example, 10 ns and we take a minimal relaxation period of say 10 lifetimes (i.e. 100 ns) we obtain an upper limit of 10 MHz. This repetition rate will be sufficient even for a confocal microscope operated in point-scanning mode. Of course the possibility of photobleaching will be an important consideration when using real samples, where thermal diffusion cannot replenish the bleached fluorophores. In this case it is vital to restrict the total irradiation dose of the sample. We are currently investigating the possibility of making a DPFLIm confocal microscope that can be used as a tool for investigating biochemistry at the molecular level.

Acknowledgment

This research was financially supported by the Stichting Technische Wetenschappen (STW), Utrecht, The Netherlands, under grant no. ANS 33.2941.

References

Anderson, S.R. (1991) Time-resolved fluorescence spectroscopy. *J. Biol. Chem.* **266,** 11405– 11408.

Brakenhoff, G.J. & Visscher, K. (1992) Confocal imaging with bilateral scanning and array detectors. *J. Microsc.* **165,** 139–146.

Brakenhoff, G.J. & Visscher, K. (1993) Imaging modes for bilateral confocal scanning microscopy. *J. Microsc.* **171,** 17–26.

Draxler, S., Lippitsch, M.E. & Leiner, M.J.P. (1993) Optical pH sensors using fluorescence decay time. *Sens. Act. B*, **11,** 421–424.

Gadella, T.W.J. Jr, Clegg, R.M. & Jovin, T.M. (1994) Fluorescence lifetime imaging microscopy: pixel-by-pixel analysis of phase-modulation data. *Bioimaging*, **2,** 139–159.

Ghauharali, R.I., Müller, M., Buist, A.H., Sosnowski, T.S., Squier, J. & Brakenhoff, G.J. (1996) Optical saturation measurements of fluorophores in solution using pulsed femtosecond excitation and two-dimensional CCD camera detection. *Appl. Opt.*, in press.

Gumy, J.-C. & Vauthey, E. (1996) Picosecond polarization grating study of the effect of excess excitation energy on the rotational dynamics of rhodamine 6G in different electronic states. *J. Phys. Chem.* **100,** 8628–8632.

Lakowicz, J.R. (1980) Fluorescence spectroscopic investigations of the dynamic properties of proteins, membranes and nucleic acids. *J. Biochem. Biophys. Methods*, **2,** 90–119.

Lakowicz, J.R. (1983) *Principles of Fluorescence Spectroscopy.* Plenum Press, New York.

Lakowicz, J.R. & Berndt, K.W. (1991) Lifetime-selective fluorescence imaging using an rf phase-sensitive camera. *Rev. Sci. Instrum.* **62** (7), 1727–1734.

Lakowicz, J.R. & Szmacinski, H. (1993) Fluorescence lifetime-based sensing of pH, Ca^{2+}, K^+ and glucose. *Sens. Act. B*, **11,** 133–143.

Lippitsch, M.E. & Draxler, S. & Leiner, M.J.P. (1992) Time-domain fluorescence methods as applied to pH sensing. *Proc. SPIE*, **1204,** 798–807.

Loudon, R. (1973) *The Quantum Theory of Light*, 2nd edn. Clarendon Press, Oxford.

Müller, M., Ghauharali, R., Visscher, K. & Brakenhoff, G.J. (1995) Double-pulse fluorescence lifetime imaging in confocal microscopy. *J. Microsc.* **177,** 171–179.

Sandison, D.R., Williams, R.M., Wells, K.S., Strickler, J. & Webb, W.W. (1995) *Handbook of Biological Confocal Microscopy* (ed. by J. B. Pawley). Plenum Press, New York.

Sanders, R., Gerritsen, H.C., Draaijer, A., Houpt, P.M. & Levine, Y.K. (1994) Fluorescence lifetime imaging of free calcium in single cells. *Bioimaging*, **2,** 131–138.

Schubert, M. & Wilhelmi, B. (1986) *Nonlinear Optics and Quantum Electronics.* John Wiley & Sons, New York.

So, P.T.C., French, T., Yu, W.M., Berland, K.M., Dong, C.Y. & Gratton, E. (1995) Time-resolved fluorescence microscopy using two-photon excitation. *Bioimaging*, **3**, 49–63.

Sosnowski, T.S., Stephens, P.B. & Norris, T.B. (1996) Production of 30-fs pulses tunable throughout the visible spectral region by a new technique in optical parametric amplification. *Opt. Lett.* **21**, 140–142.

Steiner, R.F. (1991) *Topics in Fluorescence Spectroscopy*, Vol. 2 (ed. by J. R. Lakowicz). Plenum Press, New York.

Straume, M., Frasier-Cadoret, S.G. & Johnson, M.L. (1991) *Topics in Fluorescence Spectroscopy*, Vol. 2 (ed. by J. R. Lakowicz). Plenum Press, New York.

Visscher, K., Brakenhoff, G.J. & Visser, T.D. (1994) Fluorescence saturation in confocal microscopy. *J. Microsc.* **175**, 162–165.